nature physics

ARTICLES

https://doi.org/10.1038/s41567-017-0030-7

Corrected: Publisher Correction

A quantum dipolar spin liquid

N. Y. Yao[1,2*], M. P. Zaletel[3,4], D. M. Stamper-Kurn[1] and A. Vishwanath[1,5]

Quantum spin liquids are a class of magnetic ground states reliant on non-local entanglement. Motivated by recent advances in the control of ultracold polar molecules and the development of dipolar quantum materials, we show that dipolar interactions between $S = 1/2$ moments stabilize spin liquids on the triangular and kagome lattices. In the latter case, the moments spontaneously break time-reversal, forming a chiral spin liquid with robust edge modes and emergent semions. We propose a simple route toward synthesizing a dipolar Heisenberg antiferromagnet from lattice-trapped polar molecules using only a single pair of rotational states and a constant electric field.

In strongly frustrated systems, competing interactions can conspire with quantum fluctuations to prevent classical order down to zero temperature. In an antiferromagnet, frustration allows magnetic moments to evade the formation of conventional long-range order, leading to the magnetic analogue of liquid phases. Such quantum spin liquids are characterized by long-range entanglement and can exhibit a panoply of exotic properties, ranging from emergent gauge fields and fractionalized excitations to robust chiral edge modes[1–3]. Definitively finding and characterizing such an exotic paramagnet remains one of the outstanding challenges in strongly interacting physics.

When antiferromagnetic interactions are short-ranged, frustration relies on geometry; for example, lattices containing plaquettes with an odd number of sites may frustrate Néel order. This route is most pertinent in solid-state magnets, where exchange interactions are short-ranged, and has led to the discovery of a number of exciting spin liquid candidates in layered two-dimensional Mott insulators[3–7]. An alternative route to frustration is provided by longer-range interactions[8–13]. An array of numerical studies have demonstrated that adding farther-neighbor couplings can destabilize classical order and lead to spin liquid phases; in addition, parent Hamiltonians for spin liquids have been constructed using $1/r^2$ interactions[10,13]. Unfortunately, liquid phases are often found only for a narrow range of farther-neighbor couplings comparable to the nearest-neighbour exchange, making it challenging to identify relevant physical systems.

The recent emergence of dipolar quantum materials[14–16] and polar-molecular gases opens new routes toward long-range interactions[17–20]. In contrast to both their atomic cousins and conventional quantum materials, polar molecules exhibit strong, dipolar interactions[21–23]. However, these interactions are neither isotropic nor obviously frustrated, leading to many proposals that 'engineer' frustrated phases via the use of multiple molecular states, microwave dressing fields and spatially varying optical potentials[24–29].

Furthermore, although long-ranged, the dipolar couplings are not easily fine-tuned; rather, scale invariance dictates that the simplest effective Hamiltonian one could hope for is a 'dipolar Heisenberg antiferromagnet':

$$H = \sum_{i,j} \frac{\mathbf{S}_i \cdot \mathbf{S}_j}{|R_{ij}|^3} \qquad (1)$$

Two fundamental questions arise: is H naturally realized, and what is its ground state?

Here, we answer both of these questions. First, we consider synthetic quantum magnets constructed from an array of lattice-trapped, polar molecules interacting via dipole–dipole interactions. We demonstrate that this system easily realizes the dipolar Heisenberg antiferromagnet, requiring only a judicious choice of two, undressed molecular rotational states (to represent a pseudospin) and a constant electric field[27]. The simplicity of our proposal stems from using rotational states with no angular momentum about the electric field axis. This contrasts with previous works where non-zero matrix elements appear for the transverse electric dipole operator, unavoidably generating ferromagnetic spin–spin interactions because of the inherent anisotropy of the dipolar interaction[28,29].

Second, motivated by this physical construction, we perform a large-scale density matrix renormalization group (DMRG)[30,31] study of the dipolar Heisenberg model and find evidence for quantum spin liquid ground states on both triangular and kagome lattices (Fig. 1). As a result of the long-range interactions and the need for time-reversal breaking complex wavefunctions, our model is significantly more challenging to simulate numerically than earlier nearest-neighbour models. Thus, using the infinite, translation invariant version of the algorithm, iDMRG, provides an important speed-up. The farther-neighbour dipolar couplings play a crucial role, leading to a different phase of matter for both lattice geometries when compared with their nearest-neighbour counterparts realized in Mott insulating materials. This contrasts with the case of three-dimensional classical spin ice[32]. We compute the phase diagram of the dipolar Heisenberg model as a function of experimental parameters (the electric field strength and tilt) for ultracold polar molecules.

Realization. We consider a two-dimensional array of polar molecules trapped in an optical lattice. The lattice freezes the translational motion, leaving each molecule to behave as a simple dipolar rigid rotor[25–29]. The Hamiltonian governing these molecular rotations is $H_{\mathrm{m}} = B\mathbf{J}^2 + \mathbf{E} \cdot \mathbf{d}$, where B is the rotational constant, $\mathbf{J}$ is the angular momentum operator, $\mathbf{E}$ is the external electric field and $\mathbf{d}$ is the dipole operator. For $|E|=0$, each molecule has eigenstates indexed by $|J, M\rangle$, where M is the z component of angular momentum. An applied electric field, $\mathbf{E} = E\hat{z}$, weakly aligns the molecules along the field direction, mixing states with identical M. Each $|J, M\rangle$ evolves

[1]Physics Department, University of California Berkeley, Berkeley, CA, USA. [2]Materials Science Division, Lawrence Berkeley National Laboratory, Berkeley, CA, USA. [3]Station Q, Microsoft Research, Santa Barbara, CA, USA. [4]Physics Department, Princeton University, Princeton, NJ, USA. [5]Physics Department, Harvard University, Cambridge, MA, USA. *e-mail: norman.yao@berkeley.edu

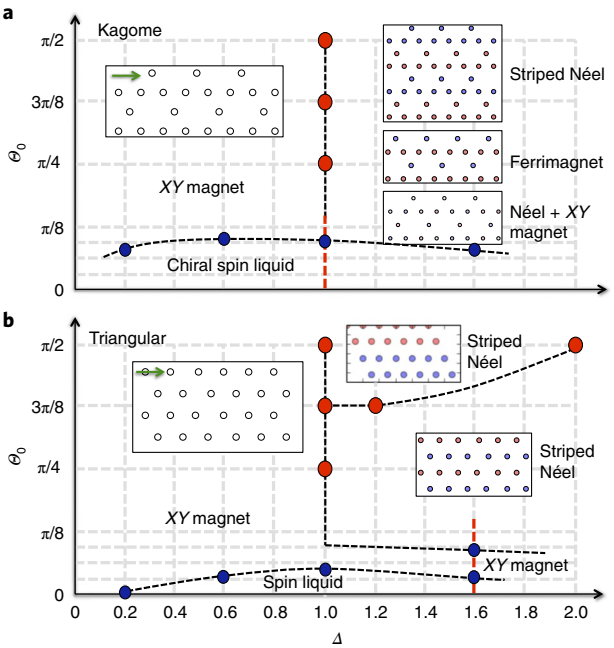

Fig. 1 | Phase diagram of the dipolar Heisenberg model. a,b, Phases on the kagome lattice (YC8 geometry truncated at J_8) (**a**) and the triangular lattice (YC6 geometry truncated at J_5) (**b**) as a function of the *XXZ* anisotropy Δ (which is controlled by the magnitude of the applied electric field (see Fig. 2)) and the polar tilt, Θ_0, of the applied electric field (the azimuthal angle is given by the green arrow). Near $\Theta_0 = 0$, where the model is fully frustrated, we observe quantum spin liquid ground states on both geometries. Ordered phases for $\Theta_0 > 0$ are shown inset with their corresponding magnetization density $\langle S_i^z \rangle$.

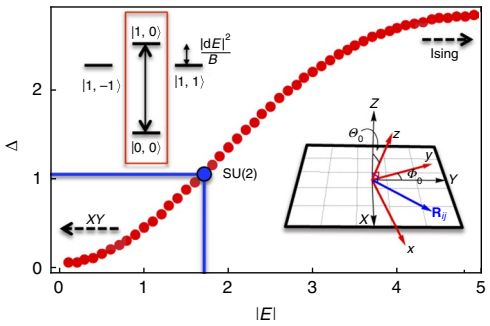

Fig. 2 | *XXZ* anisotropy as a function of electric field. The *XXZ* anisotropy Δ is controlled by the electric field strength, E, measured relative to the rotational splitting divided by the dipole moment, B/d. Top left inset: the rotational states used as the two-level pseudo-spin. Bottom right inset: molecules reside in the *XY* plane and the electric field is oriented along $\hat{z}$.

adiabatically with E, picking up a dipole moment and splitting the degeneracy within each J manifold at order $(dE)^2/B$ (inset Fig. 2).

The molecules interact with one another via the electric dipole–dipole interaction, $H_{\rm dd} = \frac{g}{2}\sum_{i\neq j}\frac{1}{R_{ij}^3}\left[\mathbf{d}_i\cdot\mathbf{d}_j - 3\left(\mathbf{d}_i\cdot\hat{\mathbf{R}}_{ij}\right)\left(\mathbf{d}_j\cdot\hat{\mathbf{R}}_{ij}\right)\right]$, where $g = 1/(4\pi\varepsilon_0)$ and $\mathbf{R}_{ij}$ is the displacement between molecules i and j. Referring to Fig. 2, we select the doublet $|\downarrow\rangle = |0,0\rangle$ and $|\uparrow\rangle = |1,0\rangle$, which are energetically resolved from all other rotational states, to play the role of a 'spin'[27]. We let S^μ denote the usual spin operators in this subspace, but note, that unlike $S = 1/2$ moments, this doublet a priori lacks SO(3) symmetry. To derive the effective Hamiltonian, we project $H_{\rm dd}$ onto the two-level subspace and drop S^z non-conserving terms as they are strongly off-resonant. This projection is physically justified by the separation of energy scales between the dipolar interaction and the rotational level-splittings: $gd^2/R^3 \ll B, (dE)^2/B$.

When the electric field is aligned perpendicular to the lattice plane (Θ_0=0, inset Fig. 2), we find[27]

$$H_{\rm eff} = g\sum_{i,j}\frac{1}{R_{ij}^3}\left[2d_{00}^2\left(S_i^xS_j^x + S_j^yS_i^y\right) + (\mu_0 - d_0)^2S_i^zS_j^z\right] \qquad (2)$$

where $d_{00} = \langle 1,0|d_z|0,0\rangle$ is the transition dipole moment, and $d_0 = \langle 0,0|d_z|0,0\rangle$ and $\mu_0 = \langle 1,0|d_z|1,0\rangle$ are the electric-field-induced 'permanent' dipole moments. The sign of the couplings shows that the interaction is antiferromagnetic along all spin axes.

As depicted in Fig. 2, the ratio $\Delta = (\mu_0 - d_0)^2/2d_{00}^2$, between the Ising and *XY* interactions (equation (2)) is controlled by the magnitude of the applied electric field. SO(3) symmetry emerges for $|dE| \approx 1.7B$, at which point the effective Hamiltonian is precisely the dipolar Heisenberg model. We note that $H_{\rm eff}$ is in stark contrast to the typical spin models analysed for polar molecules. In particular, previous works have generally considered rotational states that lead to ferromagnetic interactions favouring easy-plane (*XY*) magnetism; frustrated phases arise only on fine-tuning via microwave and optical dressing[25–29].

Ground state of the dipolar Heisenberg antiferromagnet. While long-range interactions generate frustration on any lattice, geometries with triangular motifs enhance this frustration as it is impossible for all neighbouring spins to anti-align. Here, we consider kagome and triangular lattices, both of which have been realized in optical lattices[33–35].

The ground state of the dipolar Heisenberg antiferromagnet is unknown for either lattice. Even for short-range interactions, the phase diagram in these geometries has been an open question for more than two decades, due to delicate energetic competition between many competing phases. Recently, progress has been made using DMRG[36–44]. As DMRG is a one-dimensional (1D) method, it requires mapping the 2D lattice to a quasi-1D geometry; here, we focus on infinitely long cylinders of circumference L, by using the iDMRG algorithm[31]. The dipolar interaction introduces an additional difficulty, as its range must be truncated for a consistent definition on the cylinder. Thus, our numerics require a triple extrapolation in L, the interaction range, and the accuracy of the iDMRG, which is controlled by the 'bond dimension' m. Larger m simulations are more accurate, with a computational cost that scales as m^3.

Detecting and characterizing a quantum spin liquid phase follows a decision tree. By definition, 'liquid' refers to the absence of spontaneous symmetry-breaking, specifically of spin rotations and translation invariance. Any liquid phase with half-integer spin in the unit cell must be exotic: the Hastings–Oshikawa–Lieb–Schultz–Mattis theorem requires that the phase be either a gapless spin liquid or a gapped spin liquid with fractionalized excitations[45,46]. In the gapless case, the ground state has a diverging correlation length as the circumference of the cylinder is increased. In the gapped case, the ground state will have exponentially decaying correlations, protected ground-state degeneracy and certain characteristic signatures in its entanglement spectrum[47,48].

There exists a zoo of gapped spin liquids distinguished by the braiding and statistics of their fractional excitations. The two simplest cases are the time-reversal symmetric Z_2 spin liquid and the time-reversal breaking chiral spin liquid (CSL)[2,49]; the spontaneous breaking of time-reversal is detected by using a chiral order parameter $\chi = \left\langle \mathbf{S}_i\cdot\mathbf{S}_j\times\mathbf{S}_k\right\rangle/3$, where i, j and k are the three sites of a triangle.

Let us now turn to the numerics. We refer to the cylinder geometries using the following notation[36]: YC2n is a cylinder of circumference $2n$ lattice spacings periodized along a Bravais vector (Fig. 3b,c). We emphasize that, when using the iDMRG algorithm, all cylinders are infinitely long. For both lattices, we define J_n to be the coupling between nth nearest-neighbour sites, ordered by their distance in real space, R_n. We will begin by characterizing the ground state of each lattice at the dipolar Heisenberg point and will subsequently map out the full phase diagram of the molecular proposal.

Kagome model. Extensive theoretical and numerical studies of the J_1–J_2–J_3 kagome model reveal a rich phase diagram, consisting of a honeycomb valence bond solid, a time-reversal symmetric spin liquid, a chiral spin liquid and a multitude of ordered Néel states[13,36–42,50–58]. In contrast to these previous studies, the long-range dipolar couplings cannot be tuned. For the kagome lattice, it is necessary to distinguish be tween two couplings of length $R_3=2$ lattice sites: J_3 (across hexagons) and J_3' (along bow ties) (Fig. 3b). Motivated by exchange interactions in Mott insulating materials, previous numerics have always considered $J_3'=0$. In the dipolar Heisenberg model, all couplings at a given distance are equally important and we find a finite J_3' in fact stabilizes the CSL phase (see Supplementary Information for details). This is highlighted by the fact that keeping only the J_2 or J_3 part of the dipolar interaction results in the magnetically ordered $\mathbf{q}=(0, 0)$ phase[39–42]; only upon restoring the dipolar tail of the interaction does the system transition into the CSL.

Let us now turn to the diagnostics of liquidity. We study cylinders of circumference L=8, 10 and 12 with dipolar cutoffs ranging from J_3 to J_{11}. In addition to the YC2n geometry, we also consider the so-called 'YC2n-2' geometry in which cylinders are rolled up with a 'twist' that identifies sites that differ by Bravais vector $n\mathbf{a}_1+\mathbf{a}_2$ (see the YC10-2 hashes in Fig. 3b). This convenient choice of boundary condition reduces the computational cost by decreasing the effective iDMRG unit cell by n, enabling better convergence for certain diagnostics. Crucially, neither the spin liquids nor the $\mathbf{q}=(0, 0)$ phase is frustrated by this boundary condition; more generally, for liquid phases, the resulting physics should be unaffected once the cylinder circumference is larger than the correlation length.

An advantage of the infinite-cylinder geometry is that discrete symmetries, such as translation or an Ising symmetry, can be spontaneously broken. Thus, if the phase spontaneously breaks a discrete symmetry in the 2D limit, we expect it will do so on a sufficiently large cylinder as well (as we observe in other parts of the phase diagram discussed below and in the Supplementary Information). To check that translational symmetry is preserved (that is, to rule out

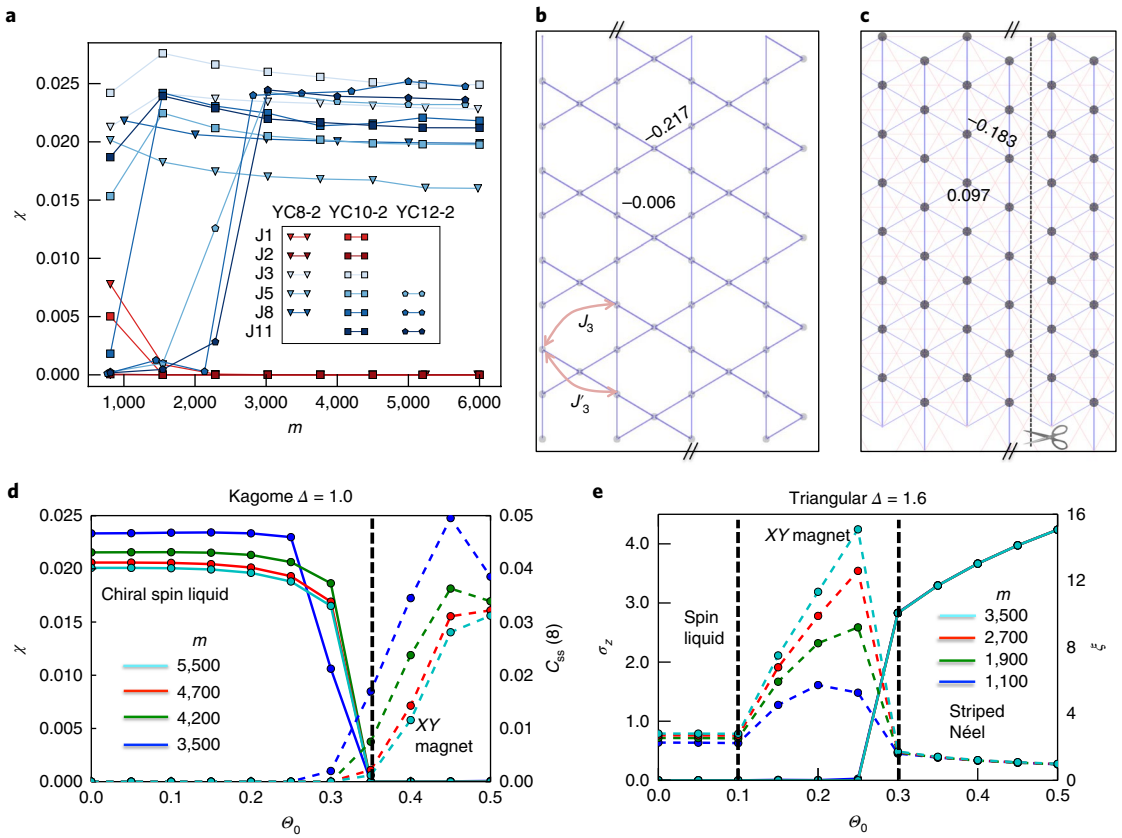

Fig. 3 | Numerical signatures of spin liquid behaviour and phase transitions. a, Triple extrapolation of the chiral order parameter χ as a function of the iDMRG bond dimension m (larger is more accurate), the cylinder circumference (L = 8, 10 or 12) and the range of the dipolar interaction (J_1–J_{11}). For YC8-2 and YC10-2, all numerics have converged to a truncation error $< 10^{-5}$, while for YC12-2, we observe a truncation error $\sim 2.9\times10^{-5}$ at bond dimension m = 6,600. **b**,**c**, The nearest-neighbour and next-nearest-neighbour $\langle \mathbf{S}_i\cdot\mathbf{S}_j\rangle$ correlations of the kagome (YC10-2)/triangle (YC8) spin liquid, respectively. The magnitude of the correlation function for each bond is shown and is directly proportional to the linewidth of the bond (see Supplementary Information for further detail). The correlations preserve the lattice symmetries, showing the absence of valence bond order. **d**, Phase transition out of the CSL (holding Δ =1.0 fixed and varying Θ_0) as characterized by the vanishing of the chiral order parameter χ (solid) and the appearance of magnetic order, observable in the spin–spin correlation function $C_{ss}(8)=\langle \mathbf{S}_i\cdot\mathbf{S}_{i+8\hat{a}_1}\rangle$ (dashed). **e**, Phase transition out of the triangular spin liquid (holding Δ = 1.6 fixed and varying Θ_0) as characterized by $\sigma_z=\frac{1}{N}\sum_i\langle S_i^z\rangle^2$, the variance in magnetization across the unit cell (solid) and the correlation length ξ (dashed).

valence-bond order), we verify that the bond correlations are translation invariant (Fig. 3b) and also calculate the overlap of the ground state, $|\Psi\rangle$, with a translated version ofitself, $\langle\Psi|\widehat{T}^{y}|\Psi\rangle=(1-\varepsilon)^{V}$. This overlap scales with the volume of the system, V, with error $\varepsilon<0.004$. The above are quoted for a YC10 geometry with couplings up to J_8, but similar results are found when truncating to J_3 or extending to J_{11}, as well as on the smaller YC8 geometry and the larger YC12-2 geometry (see the Supplementary Information for details, and for comparison with a known valence-bond solid state).

While discrete symmetries can be spontaneously broken, Néel order that breaks a continuous symmetry is ruled out by the Mermin–Wagner theorem in our quasi-1D geometry, and we indeed find $\langle S_i^{\mu}\rangle\to 0$ as the iDMRG accuracy m is increased. In our diagnostics, a tendency toward Néel order will instead appear as algebraic correlations beyond the dipolar cutoff, or a correlation length that diverges with cylinder circumference. To ensure that this is not the case, we employ two additional quantitative and qualitative tests, namely, by checking for the absence of algebraic ordering at fixed circumference and the absence of increasing long-range order as the cylinder circumference increases. Indeed, we find an extremely short correlation length $\xi\lesssim 0.9a$ (as calculated from the iDMRG transfer matrix) that does not significantly increase with the iDMRG accuracy or cylinder circumference (see Supplementary Information for details), consistent with a gapped paramagnet. Moreover, the absence of long-range correlations (Fig. 3) indicates that spin rotation symmetry is also preserved. By stark contrast, when the interaction is truncated to J_1, J_2, we observe clear long-range order, and the resulting correlations are qualitatively distinct, as shown in the Supplementary Information.

A key requirement for the CSL phase is the spontaneous breaking of time-reversal symmetry. To this end, the chiral order parameter $|\chi|$ is shown in Fig. 3a as a function of the size of the cylinder, the cutoff of the dipolar interaction and the iDMRG accuracy; $|\chi|$ increases weakly with cylinder circumference, converges with the DMRG accuracy m and saturates for large dipolar cutoff.

In addition to spontaneous time-reversal breaking, the most spectacular signature of a CSL is a chiral edge state. Quantum entanglement provides a way to probe these edge states given only the ground state. The reduced density matrix ρ_{L} for half of the cylinder can be viewed as a thermal density matrix of a semi-infinite cylinder, introducing a single 'edge'. The spectrum $p_{\mathrm{a}}=e^{-E_{\mathrm{a}}}$ of ρ_{L} (that is, the 'entanglement spectrum') is known to mimic the energy spectrum E_{a} of the physical edge[47,59,60]. On YC2n, the entanglement cut runs parallel to the Bravais vector $n\mathbf{a}_1$ used to compactify the cylinder (scissors in Fig. 3c), so that ρ_{L} preserves the rotational symmetry of the cylinder, allowing us to assign a corresponding momentum $k_{\mathrm{a}}\in\frac{2\pi m}{n}$ to each level. Plotting E_{a} versus the momenta k_{a} should reveal a chiral dispersion relation. As shown in Fig. 4a,b, there is a low-lying set of levels dispersing rightward, roughly as $E_{\mathrm{a}}\sim vka$. Focusing on the levels with $S^z=0$, the number of levels at each momenta k follows the level counting $\{1,1,2,3,5\cdots\}$; these are the partitions of integers expected when occupying a set of bosonic edge modes $b_k^{\dagger}, k>0$. Each level is in fact an SO(3) multiplet, consistent with the $\mathrm{SU}(2)_1$ Wess–Zumino–Witten edge theory[55,61]. Furthermore, we find a second degenerate ground state (analogous to the expected two-fold topological degeneracy of a CSL on a torus), whose entanglement spectrum is consistent with the semion sector of the CSL[55]. Note that a right-moving spectrum spontaneously breaks time-reversal; when the iDMRG is initialized differently, right- and left-moving spectra appear with equal probability.

Triangular model. We now turn to the triangular lattice. Truncating the dipolar Heisenberg model at short range leads to Néel order: for J_1 only, a 120° Néel phase[62], and for J_1, J_2, a two-sublattice collinear Néel phase[43,44]. However, adding in the dipolar J_3 coupling directly penalizes the order of the collinear state and appears to drive the system into a liquid; this is evidenced by a drastic change in the $\langle S_i\cdot S_j\rangle$ correlation function as the long-range tail of the interaction is restored (see Supplementary Information). With couplings through J_5, the YC8 ground state has an XY correlation length of $\xi\lesssim 1.4a$ and is translationally symmetric with $\varepsilon<4\times10^{-5}$. Similar results are found when truncating to J_3 or extending to J_8, as well as on the smaller YC6 geometry and the larger YC10 geometry.

The phenomenology of the observed spin liquid phase is equivalent to the J_1–J_2 spin liquid reported previously[43,44,56,63]. The lowest energy state is time-reversal symmetric and has an entanglement spectrum consistent with the fermionic spinon topological sector of a Z_2 or U(1) spin liquid[54,56]; it exhibits a four-fold degeneracy and a half-integral representation of SO(3) as shown in Fig. 4[48]. While the bond correlations are translation invariant (Fig. 3c), they exhibit a noticeable striping consistent with nematic ordering (note that this nematicity may be an artefact of the cylindrical geometry that breaks C_6 symmetry)[43]. The nature of this triangular spin liquid is not yet fully understood.

Phase diagram. The above results (for both triangular and kagome) were presented for the SO(3) symmetric Heisenberg antiferromagnet ($\Delta=1$) at $|dE|\approx 1.7B$. For both stronger ($\Delta=1.6$) and weaker ($\Delta=0.6$) electric fields, the SO(3) model is broken down to a U(1) XXZ model, but our numerics find that the spin liquid phases are completely consistent with those observed at the SO(3) point[42]. Note that the Hastings–Oshikawa–Lieb–Schultz–Mattis theorem requires only U(1) invariance about the z axis and zero net magnetization.

As one tilts the electric field into the lattice plane, the spin liquids we observe begin to compete with magnetically ordered phases. The tilt generates angular dependence in the effective Hamiltonian,

$$H_{\mathrm{eff}}=g\sum_{i,j}\frac{1}{R_{ij}^{3}}[1-3\cos^2(\Phi-\Phi_0)\sin^2\Theta_0]\times\left[2d_{00}^2\left(S_i^xS_j^x+S_j^yS_i^y\right)+(\mu_0-d_0)^2S_i^zS_j^z\right] \quad (3)$$

where Φ and Φ_0 are the polar angles of $\mathbf{R}_{ij}$ and the electric field orientation, respectively (inset of Fig. 2). For non-zero Θ_0, full frustration is lost as dipoles begin to point head-to-tail along the field direction, thereby exhibiting ferromagnetic interactions. For large Θ_0, a variety of ordered phases appear as shown in Fig. 1a,b (for more details, see Supplementary Information). Here, we restrict our interest to the phase boundaries of the spin liquid states.

In Fig. 3d,e, we present two representative vertical cuts: out of the kagome CSL at $\Delta=1.0$, and out of the triangular spin liquid at $\Delta=1.6$. In the kagome case, we identify the transition out of the CSL via the vanishing of the chiral order parameter (Fig. 3d). In the triangular case, we diagnose the phase transition by examining the correlation length and the variance of the S^z magnetization (Fig. 3e). This reveals two phases, an XY magnet directly proximate to the spin liquid and the expected striped Néel phase for larger Θ_0. In addition to showing that the spin liquid phases persist to moderate electric field tilts, understanding the nature of the ordered phases surrounding the spin liquids may enable the adiabatic preparation of these topological states[64]; such preparation may benefit from utilizing molecules with larger dipole moments (since our approach is generic to all bi-alkali polar molecules), enabling preparation on faster timescales. An alternative route for preparation—natural in the context of optical lattices—is to utilize a bilayer geometry where one layer plays the role of an entropy/energy sink and 'cools' the adjacent layer (see Supplementary Information for more details). This specific approach is particularly simple in systems with long-range interactions such as polar molecules, whereby decreasing the

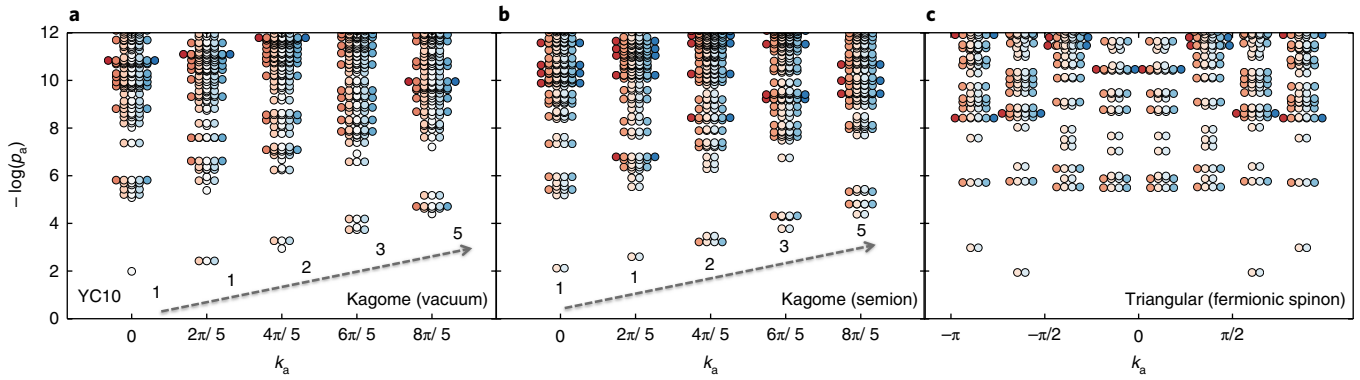

Fig. 4 | Entanglement spectra. The entanglement spectrum $\{p_a\}$ as a function of $k_a \in \frac{2\pi n}{L_y}$, the momentum of the entanglement state around the cylinder. Data points are coloured and displaced slightly according to their S^z quantum numbers. Note that k is periodic modulo 2π, so all the allowed momenta are shown here. **a**, The kagome YC10 model truncated at J_8. The levels have right-moving chiral dispersion, implying that time-reversal is broken. The momentum-resolved entanglement spectrum is consistent with the vacuum sector of a CSL and exhibits the characteristic counting $\{1, 1, 2, 3, \cdots\}$ predicted by the chiral edge theory, with S^z taking integer values (for example, $S^z = 0$ is centred). **b**, Entanglement spectrum of the second, degenerate YC10 ground state, which corresponds to the semion sector of the CSL; all levels are two-fold degenerate, consistent with half-integral representations of SO(3) (for example, $S^z = \pm 1/2$)[72]. **c**, The triangular YC8 model truncated at J_5. The spectrum is consistent with the fermionic spinon topological sector of a Z_2 or U(1) spin liquid.

density of particles in the sink layer naturally enables it to behave as a coolant[65]. However, even before ground-state cooling, one must first prepare the system in the zero-magnetization manifold of the molecular pseudo-spin states; a particularly simple approach is to perform a uniform $\pi/2$ pulse starting from the $|\downarrow\rangle = |0, 0\rangle$ state. While elegant, this approach exhibits intrinsic $\sqrt{N}$ magnetization fluctuations, which should be unimportant for sufficiently large numbers of molecules (a number of alternative initialization techniques that do not exhibit magnetization fluctuations are also detailed in the Supplementary Information).

We note that realizing a gapped spin liquid such as the kagome CSL affords some flexibility in the required lattice filling fraction[66]. In particular, the chiral spin liquid will tolerate some amount of lattice dilution: each vacancy will be 'screened' by a spinon, preserving the spin gap. Only at some critical dilution will the spin liquid order be destroyed. A rough estimate of this critical dilution is when the inter-vacancy distance is comparable to the correlation length $\xi \sim 1$ lattice site, suggesting that our observed CSL phase may remain robust to ~10% dilution.

Once prepared, there are a number of approaches to detecting the CSL based on either spontaneous or stimulated Bragg scattering[67]. In addition to revealing the spin excitation gap, the fractionalization of a single 'spin' flip into a pair of spinon excitations would be captured by the shape of the spectral line. In particular, rather than observing a sharp magnon mode, one expects to observe a broad spectrum, reflecting the two-spinon continuum. Moreover, the onset of the spin-excitation spectrum near the gap also shows signatures of quasiparticle self-braiding, exhibiting a functional power law whose exponent captures the semionic statistics of the chiral spin liquid phase[68].

In summary, our proposal provides a new route toward studying frustrated quantum magnetism in an ultracold lattice gas. The dipolar Heisenberg antiferromagnet exhibits promising signs of spin liquid behaviour on both the kagome and triangular lattices, distinct from models of nearest-neighbour exchange. In addition to lattice trapped molecules, long-range Heisenberg antiferromagnets may also be found in designer magnetic lattices[69,70] as well as dipolar quantum materials[14–16]. Looking forward, it is important to consider the effects of lattice vacancies and dipolar relaxation as well as to identify unique signals of frustration in quench dynamics. It would also be of interest to consider higher-spin models, which may host non-Abelian phases[71].

Data availability. The data that support the plots within this paper and other findings of this study are available from the corresponding author upon request.

Received: 11 January 2016; Accepted: 4 December 2017;
Published online: 5 February 2018

References

1. Anderson, P. Resonating valence bonds: A new kind of insulator? *Mater. Res. Bull.* **8**, 153 (1973).
2. Kalmeyer, V. & Laughlin, RB. Equivalence of the resonating-valence-bond and fractional quantum Hall states. *Phys. Rev. Lett.* **59**, 2095 (1987).
3. Balents, L. Spin liquids in frustrated magnets. *Nature* **464**, 199 (2010).
4. Shimizu, Y., Miyagawa, K., Kanoda, K., Maesato, M. & Saito, G. Spin liquid state in an organic Mott insulator with a triangular lattice. *Phys. Rev. Lett.* **91**, 107001 (2003).
5. Itou, T., Oyamada, A., Maegawa, S., Tamura, M. & Kato, R. Quantum spin liquid in the spin-1/2 triangular antiferromagnet $EtMe_3Sb[Pd(dmit)_2]_2$. *Phys. Rev. B* **77**, 104413 (2008).
6. Rigol, M. & Singh, R. R. P. Magnetic susceptibility of the kagome antiferromagnet $ZnCu_3(OH)_6Cl_2$. *Phys. Rev. Lett.* **98**, 207204 (2007).
7. Helton, J. S. et al. Spin dynamics of the spin-1/2 kagome lattice antiferromagnet $ZnCu_3(OH)_6Cl_2$. *Phys. Rev. Lett.* **98**, 107204 (2007).
8. Harris, M. J., Bramwell, S. T., McMorrow, D. F., Zeiske, T. & Godfrey, K. W. Geometrical frustration in the ferromagnetic pyrochlore $Ho_2Ti_2O_7$. *Phys. Rev. Lett.* **79**, 2554 (1997).
9. Castelnovo, C., Moessner, R. & Sondhi, S. L. Magnetic monopoles in spin ice. *Nature* **451**, 42–45 (2008).
10. Thomale, R., Kapit, E., Schroeter, D. F. & Greiter, M. Parent Hamiltonian for the chiral spin liquid. *Phys. Rev. B* **80**, 104406 (2009).
11. Taroni, A. & Hjörvarsson, B. Influence of the range of interactions in thin magnetic structures. *Eur. Phys. J. B* **77**, 367 (2010).
12. Kraemer, C. et al. Dipolar antiferromagnetism and quantum criticality in $LiErF_4$. *Science* **336**, 1416–1419 (2012).
13. Greiter, M., Schroeter, D. F. & Thomale, R. Parent Hamiltonian for the non-Abelian chiral spin liquid. *Phys. Rev. B* **89**, 165125 (2014).
14. Shen, S.-P. et al. Quantum electric-dipole liquid on a triangular lattice. *Nat. Commun.* **7**, 10569 (2016).
15. Hassan, N. et al. Observation of a quantum dipole liquid state in an organic quasi-two-dimensional material. Preprint at: https://arxiv.org/abs/1704.04482 (2017).
16. Shimozawa, M. et al. Quantum-disordered state of magnetic and electric dipoles in an organic Mott system. *Nat. Commun.* **8**, 1821 (2017).
17. Ni, K.-K. et al. A high phase-space-density gas of polar molecules. *Science* **322**, 231–235 (2008).
18. Chotia, A. et al. Long-lived dipolar molecules and Feshbach molecules in a 3D optical lattice. *Phys. Rev. Lett.* **108**, 080405 (2012).

19. Deiglmayr, J. et al. Formation of ultracold polar molecules in the rovibrational ground state. *Phys. Rev. Lett.* **101**, 133004 (2008).
20. Park, J. W., Will, S. A. & Zwierlein, M. W. Ultracold dipolar gas of fermionic $^{23}Na^{40}K$ molecules in their absolute ground state. *Phys. Rev. Lett.* **114**, 205302 (2015).
21. Yan, B. Observation of dipolar spin-exchange interactions with lattice-confined polar molecules. *Nature* **501**, 521–525 (2013).
22. Hazzard, K. R. et al. Many-body dynamics of dipolar molecules in an optical lattice. *Phys. Rev. Lett.* **113**, 195302 (2014).
23. Baranov, M., Dalmonte, M., Pupillo, G. & Zoller, P. Condensed matter theory of dipolar quantum gases. *Chem. Rev.* **112**, 5012–5061 (2012).
24. Lewenstein, M. Atomic and molecular physics: Polar molecules in topological order. *Nat. Phys.* **2**, 309–310 (2006).
25. Micheli, A., Brennen, G. & Zoller, P. A toolbox for lattice-spin models with polar molecules. *Nat. Phys.* **2**, 341–347 (2006).
26. Gorshkov, A. V. et al. Tunable superfluidity and quantum magnetism with ultracold polar molecules. *Phys. Rev. Lett.* **107**, 115301 (2011).
27. Gorshkov, A. V. et al. Quantum magnetism with polar alkali-metal dimers. *Phys. Rev. A* **84**, 033619 (2011).
28. Yao, N. Y. et al. Realizing fractional Chern insulators in dipolar spin systems. *Phys. Rev. Lett.* **110**, 185302 (2013).
29. Manmana, S. R. et al. Topological phases in ultracold polar-molecule quantum magnets. *Phys. Rev. B* **87**, 08110(R)6 (2013).
30. White, S. R. Density matrix formulation for quantum renormalization groups. *Phys. Rev. Lett.* **69**, 2863 (1992).
31. McCulloch, I. P. Infinite size density matrix renormalization group, revisited. Preprint at: https://arxiv.org/abs/0804.2509 (2008).
32. Isakov, S. V., Moessner, R. & Sondhi, S. Why spin ice obeys the ice rules. *Phys. Rev. Lett.* **95**, 217201 (2005).
33. Jo, G.-B. et al. Ultracold atoms in a tunable optical kagome lattice. *Phys. Rev. Lett.* **108**, 045305 (2012).
34. Becker, C. et al. Ultracold quantum gases in triangular optical lattices. *New J. Phys.* **12**, 065025 (2010).
35. Struck, J. et al. Quantum simulation of frustrated classical magnetism in triangular optical lattices. *Science* **333**, 996–999 (2011).
36. Yan, S., Huse, D. A. & White, S. R. Spin-liquid ground state of the $S = 1/2$ kagome Heisenberg antiferromagnet. *Science* **332**, 1173–1176 (2011).
37. Depenbrock, S., McCulloch, I. P. & Schollwöck, U. Nature of the spin-liquid ground state of the S=1/2 Heisenberg model on the kagome lattice. *Phys. Rev. Lett* **109**, 067201 (2012).
38. Jiang, H.-C., Wang, Z. & Balents, L. Identifying topological order by entanglement entropy. *Nat. Phys.* **8**, 902–905 (2012).
39. Gong, S.-S., Zhu, W., Balents, L. & Sheng, D. N. Global phase diagram of competing ordered and quantum spin-liquid phases on the kagome lattice. *Phys. Rev. B* **91**, 075112 (2015).
40. He, Y. C., Sheng, D. & Chen, Y. Chiral spin liquid in a frustrated anisotropic kagome Heisenberg model. *Phys. Rev. Lett.* **112**, 137202 (2014).
41. Gong, S.-S., Zhu, W. & Sheng, D.N. Emergent chiral spin liquid: fractional quantum Hall effect in a kagome Heisenberg model. *Sci. Rep.* **4**, 6317 (2014).
42. He, Y.-C. & Chen, Y. Distinct spin liquids and their transitions in spin-1/2 XXZ kagome antiferromagnets. *Phys. Rev. Lett.* **114**, 037201 (2015).
43. Zhu, Z. & White, S. R. Spin liquid phase of the S=½J_1–J_2 Heisenberg model on the triangular lattice. *Phys. Rev. B* **92**, 04110(R)5 (2015).
44. Hu, W.-J., Gong, S.-S., Zhu, W. & Sheng, D. Competing spin-liquid states in the spin-½ Heisenberg model on the triangular lattice. *Phys. Rev. B* **92**, 140403(R) (2015).
45. Oshikawa, M. Commensurability, excitation gap, and topology in quantum many-particle systems on a periodic lattice. *Phys. Rev. Lett* **84**, 1535 (2000).
46. Hastings, M. B. Sufficient conditions for topological order in insulators. *Europhys. Lett.* **70**, 824 (2005).
47. Kitaev, A. & Preskill, J. Topological entanglement entropy. *Phys. Rev. Lett.* **96**, 110404 (2006).
48. Zaletel, M., Lu, Y.-M. & Vishwanath, A. Measuring space-group symmetry fractionalization in Z_2 spin liquids. *Phys. Rev. B* **96**, 195164 (2017).
49. Wen, X. G., Wilczek, F. & Zee, A. Chiral spin states and superconductivity. *Phys. Rev. B* **39**, 11413 (1989).
50. Singh, R. R. & Huse, D. A. Ground state of the spin-1/2 kagome-lattice Heisenberg antiferromagnet. *Phys. Rev. B* **76**, 180407(R) (2007).
51. Nakano, H. & Sakai, T. Numerical-diagonalization study of spin gap issue of the kagome lattice Heisenberg antiferromagnet. *J. Phys. Soc. Jpn* **80**, 053704 (2011).
52. Läuchli, A. M., Sudan, J. & Sørensen, E. S. Ground-state energy and spin gap of spin-1/2 Kagomé-Heisenberg antiferromagnetic clusters: large-scale exact diagonalization results. *Phys. Rev. B* **83**, 212401 (2011).
53. Messio, L., Bernu, B. & Lhuillier, C. Kagome antiferromagnet: A chiral topological spin liquid? *Phys. Rev.Lett.* **108**, 207204 (2012).
54. Iqbal, Y., Becca, F., Sorella, S. & Poilblanc, D. Gapless spin-liquid phase in the kagome spin-1/2 Heisenberg antiferromagnet. *Phys. Rev. B* **87**, 060405(R) (2013).
55. Bauer, B. et al. Nonlinear spin-wave excitations at low magnetic bias fields. *Nat. Commun.* **5**, 8274 (2014).
56. He, Y.-C., Zaletel, M. P., Oshikawa, M. & Pollmann, F. Signatures of Dirac cones in a DMRG study of the kagome Heisenberg model. *Phys. Rev. X* **7**, 031020 (2017).
57. Liao, H. et al. Gapless spin-liquid ground state in the S=1/2 kagome antiferromagnet. *Phys. Rev. Lett.* **118**, 137202 (2017).
58. Sakai, T. & Nakano, H. Gapless quantum spin liquid of the kagome-lattice antiferromagnet. *Polyhedron* **126**, 42–44 (2017).
59. Li, H. & Haldane, F. Entanglement spectrum as a generalization of entanglement entropy: Identification of topological order in non-Abelian fractional quantum Hall effect states. *Phys. Rev. Lett.* **101**, 010504 (2008).
60. Qi, X.-L., Katsura, H. & Ludwig, A. W. W. General relationship between the entanglement spectrum and the edge state spectrum of topological quantum states. *Phys. Rev. Lett.* **108**, 196402 (2012).
61. Wess, J. & Zumino, B. Consequences of anomalous ward identities. *Phys. Lett. B* **37**, 95 (1971).
62. Jolicoeur, T., Dagotto, E., Gagliano, E. & Bacci, S. Ground-state properties of the S=1/2 Heisenberg antiferromagnet on a triangular lattice. *Phys. Rev. B* **42**, 4800(R) (1990).
63. Saadatmand, S. N. & McCulloch, I. P. Symmetry fractionalization in the topological phase of the spin-½J_1–J_2 triangular Heisenberg model. *Phys. Rev. B* **94**, 1211 11(R) (2016).
64. Barkeshli, M., Yao, N. Y. & Laumann, C. R. Continuous preparation of a fractional Chern insulator. *Phys. Rev. Lett.* **115**, 026802 (2015).
65. Zaletel, M. P., Stamper-Kurn, D. M. & Yao, N. Y. Preparation of low entropy correlated many-body states via conformal cooling quenches. Preprint at: https://arxiv.org/abs/1611.04591 (2016).
66. Moses, S. A. et al. Creation of a low-entropy quantum gas of polar molecules in an optical lattice. *Science* **350**, 659–662 (2015).
67. Ernst, P. T. et al. Probing superfluids in optical lattices by momentum-resolved Bragg spectroscopy. *Nat. Phys.* **6**, 56–61 (2010).
68. Morampudi, S. C., Turner, A. M., Pollmann, F. & Wilczek, F. Statistics of fractionalized excitations through threshold spectroscopy. *Phys. Rev. Lett.* **118**, 227201 (2017).
69. Yao, N. Y., Glazman, L. I., Demler, E. A., Lukin, M. D. & Sau, J. D. Enhanced antiferromagnetic exchange between magnetic impurities in a superconducting host. *Phys. Rev. Lett.* **113**, 087202 (2014).
70. Kezilebieke, S., Dvorak, M., Ojanen, T. & Liljeroth, P. Coupled Yu–Shiba–Rusinov states in moleculardimers on NbSe. Preprint at: https://arxiv.org/abs/1701.03288 (2017).
71. Greiter, M. & Thomale, R. Non-Abelian statistics in a quantum antiferromagnet. *Phys. Rev. Lett* **102**, 207203 (2009).
72. Zaletel, M. P., Zhu, Z., Lu, Y.-M., Vishwanath, A. & White, S. R. Space group symmetry fractionalization in a chiral kagome Heisenberg antiferromagnet. *Phys. Rev. Lett* **116**, 197203 (2016).

Acknowledgements

We gratefully acknowledge the insights of and discussions with B. Lev, A. Gorshkov, A. M. Rey, M. Lukin, C. Laumann, J. Moore, R. Thomale, J. Ye and M. Zwierlein. This work was supported by the AFOSR MURI grant FA9550-14-1-0035, the NSF (grant no. PHY-1654740), the Miller Institute for Basic Research in Science, the LDRD Program of LBNL under US DOE Contract No. DE-AC02-05CH11231, and the Simons Investigators programme.

Author contributions

All authors contributed extensively to all aspects of this work.

Competing interests

The authors declare no competing financial interests.

Additional information

Supplementary information is available for this paper at https://doi.org/10.1038/s41567-017-0030-7.

Reprints and permissions information is available at www.nature.com/reprints.

Correspondence and requests for materials should be addressed to N.Y.Y.

Publisher's note: Springer Nature remains neutral with regard to jurisdictional claims in published maps and institutional affiliations.